Mapping Tree Species in Coastal Portugal Using Statistically Segmented Principal Component Analysis and Other Methods

Prem Chandra Pandey, *Member, IEEE*, Nicholas J. Tate, and Heiko Balzter

***Abstract*— Hyperspectral sensors record radiances in a large number of wavelengths of the electromagnetic spectrum and can be used to distinguish different tree species based on their characteristic reflectance signatures. Reflectance spectra were measured from airborne hyperspectral AISA Eagle/Hawk imagery in order to identify different Mediterranean tree species at a coastal test site in Portugal. A spectral range from 400 to 2450 nm was recorded at 2-m spatial resolution. The hyperspectral data are divided into five spectral data ranges. The chosen ranges for segmentation are based on statistical properties as well as on their wavelengths, as radiances of a particular wavelength may overlap with neighboring wavelengths. Principal component analysis (PCA) is applied individually to each spectral range. The first three principal components (PCs) of each range are chosen and are fused into a new data segment of reduced dimensionality. The resulting 15 PCs contain 99.42% of the information content of the original hyperspectral image. These PCs were used for a maximum likelihood classification (MLC). Spectral signatures were also analyzed for the hyperspectral data, and were validated with ground data collected in the field by a handheld spectro-radiometer. Different RGB combinations of PC bands of segmented PC image provide distinct feature identification. A comparison with other classification approaches (spectral angle mapper and MLC of the original hyperspectral imagery) shows that the MLC of the segmented PCA achieves the highest accuracy, due to its ability to reduce the Hughes phenomenon.**

***Index Terms*— Hyperspectral remote sensing, segmented principal component analysis, maximum likelihood classification, spectral angle mapper, forest mapping, ground data, coastal vegetation.**

I. Introduction

HYPERSPECTRAL images provide the potential for more accurate and detailed spectral information extraction compared to other types of remotely sensed data, due to their large number of spectral bands. Researchers have successfully used hyperspectral imagery to map vegetation species [1], invasive species [2], above-ground biomass [3], environmental parameters [4] and vegetation stress and disease [5]. Previous studies show that multi-sensor approaches have been used to discriminate tree species for forest management using techniques such as spectral reflectance [6], Support Vector Machines (SVM) [7], MLC and SAM [8]. Over the past decades, different classification techniques have been developed for hyperspectral data [9]. They were compared for applications to land use / land cover mapping and other remote sensing purposes and MLC has been considered as superior to other classifier approaches [10]–[12]. MLC is based on the class probability density functions assuming a multivariate normal distribution and often achieves more accurate results than other methods [13]. MLC is available in most software packages like ENVI©, Arc GIS®, ERDAS Imagine® [14], [15].

The high spectral resolution and large number of spectral bands of hyperspectral images enable a better identification of land use / land cover types [16], [17] as well as other features like vegetation type, crop type and soils [15], [18]. Hyperspectral imaging enables an effective mapping of vegetation in diverse environments like estuaries [19], marshland [20] and tropical rainforest [21]. However, the high data volume and dimensionality of hyperspectral data is a constraint for information extraction due to long processing times [22]. This needs to be resolved using compression techniques to reduce the dimensionality of the data while retaining enough of the original spectral information [22]–[24]. In digital image processing, PCA is commonly used for image compression. It performs a multidimensional coordinate system rotation to convert the original inter-correlated bands into a new set of uncorrelated PCs where a small number of PCs contains most of the variation. Karathanassi [25] described PCA as a mathematically rigorous technique where the original spectral information is retained. Segmented PCA was developed to reduce the 'Hughes phenomenon', which means that by adding more spectral bands to a standard MLC the classification result eventually becomes less accurate [22], [26]. Too many input bands can thus lead to a degradation of the classified map. Bellman [27] investigated the relationship between the number of bands and the number of training samples for image classification and termed it the 'curse of dimensionality' due to the rapid increase in required training samples for density estimation. As dimensionality increases with the number of bands, the number of training samples needed for

Manuscript received May 15, 2014; revised June 23, 2014; accepted June 24, 2014. Date of publication July 8, 2014; date of current version October 23, 2014. The work of P. C. Pandey was supported by the Association of Commonwealth Universities (INCS-2011-155 Commonwealth Fellowship). The work of H. Balzter was supported by the Royal Society Wolfson Research Merit Award, 2011/R3. The associate editor coordinating the review of this paper and approving it for publication was Prof. Octavian Postolache.

P. C. Pandey and H. Balzter are with the Centre for Landscape and Climate Research, Department of Geography, University of Leicester, Leicester LE1 7RH, U.K. (e-mail: prem26bit@gmail.com; pcp6@le.ac.uk; hb91@le.ac.uk).

N. J. Tate is with the Department of Geography, University of Leicester, Leicester LE1 7RH, U.K. (e-mail: njt9@le.ac.uk).

Color versions of one or more of the figures in this paper are available online at http://ieeexplore.ieee.org.

Digital Object Identifier 10.1109/JSEN.2014.2335612

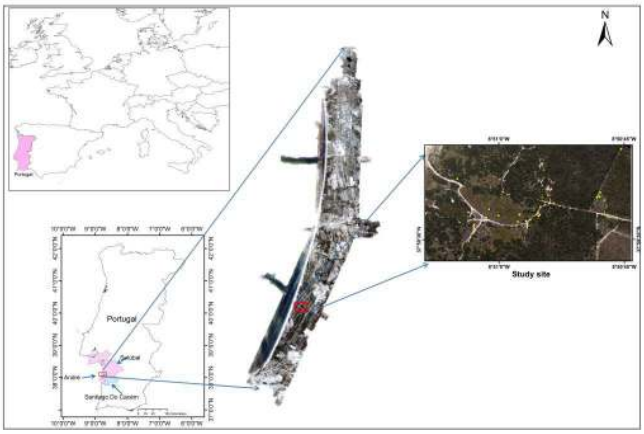

Fig. 1. Location map of the study site. The yellow circles shown in the study site were the few ground points collected with GPS during field survey.

a classifier should increase exponentially [28], [29]. Thus, in the classifier design it leads to ambiguity in the classification, where the classification accuracy increases and then declines with an increasing number of bands, while keeping the training samples constant [28]–[31]. The 'Hughes phenomenon' cannot be prevented unless providing a sufficiently large number of samples. Thus bringing high order dimensionality to a lower order will reduce the 'Hughes phenomenon' [32] by applying the PCA technique [33]. Here, a segmented PCA was applied to reduce the 'Hughes phenomenon', which computes the maximum data variance and generates uncorrelated bands.

II. Study Area

The study site is located in the western part of Portugal. It is a long coastal strip of 3 km × 5 km at St. André, in Setubal, Portugal (Figure 1). The study area has a spatial extent between 8°49'38.79"W and 8°51'2.14"W and between 37°59'12.46"N and 37°59'35.02"N. This coastal strip has a diverse topography with protected forests, freshwater lagoons, and dry sand dune vegetation. Portuguese forests are characteristic for the Mediterranean climate, and they represent high species richness and unique native species [34]. Mediterranean forests typically have broadleaved trees such as Oak (evergreen and deciduous *Quercus* species) and *Eucalyptus globulus* with frequent conifers like *Pinus pinea, Pinus pinaster* etc. Alien species like *Acacia longifolia* (also called Sydney Golden Wattle), which was introduced to stabilize the sand dunes, can become dominant due to its invasive nature.

Mediterranean forests are characterized by hot and dry summers and mild, rainy winters, with nearly all rainfall occurring in the winter and spring. They occur in five Mediterranean climate zones on the west coast of continents in the mid-latitudes (30°-45°N or S) and occupy less than 5% of the Earth's surface [35]. Mediterranean forests are found in low-lying plains along the coastal regions. The typical vegetation is influenced by the Mediterranean climate but also affected by altitude [34]. Summer weather often leads to conditions favorable to forest fires. Thus, forest mapping plays a very important role in forest management and tree species protection, as well as deforestation and afforestation monitoring.

III. Data and Methodology Used

The data were acquired by NERC (National Environment Research Council- EUFAR11/06 project) for the European Facility for Airborne Research (EUFAR). The flight campaign was in April 2011 in mid-day. Hyperspectral data were captured using AISA (Airborne Imaging Spectrometer for Applications), Hawk and Eagle sensors by Specim. AISA has dual sensors for acquiring data while Eagle has a wavelength range from 400 nm to 970 nm and Hawk from 970 nm to 2450 nm. These latter two sensor systems collected data in 492 narrow spectral bands simultaneously [36]. During the acquisition of the hyperspectral images, airborne Lidar data were also collected. Lidar data were used for the generation of a digital elevation model (DEM) in combination with ASTER data for geometric correction with the *apl* software suite. The *apl* software contains three components – *apl corr*, *apl tran* and *apl map* which generate calibrated, geo referenced, roll, pitch and yaw corrected hyperspectral imagery. *apl corr* was designed for calibration from level 1 to level 2b with a DEM (generated using Lidar and Aster data). Level 2b can be geo-corrected with *apl tran* and mapped to a regular grid for level 3b using *apl map*.

Topographic maps of scale 1:25,000 and digital photographs were used as auxiliary tools in the definition of training classes and in the validation. The collection of spatial information on land cover classes, roads and ground control points (GCP) was performed by GPS during a field visit to the study site in September 2012. A total of 70 points of tree species including *Pinus pinea, Pinus pinaster, Eucalyptus globulus, Acacia longifolia* and other classes were recorded. Of these, 35 points were used for training of the classification and the other 35 for validation of the results. The GCPs were collected at intersecting corners of visible land cover parcel boundaries and other features that can be identified reliably in the images [37].

A. Data Processing Steps

The conceptual framework of the research followed 6 main steps: geometric correction, atmospheric correction, image enhancement, image transformation (segmented PCA), classification and interpretation and validation of the results. Image processing and analysis were carried out with *apl* and ENVI 4.7 and GIS analysis with ArcGIS 10. The hyperspectral data were delivered as radiometrically calibrated Level 1b products and were processed to level 3b using the NERC-ARSF *apl* software [38]. A schematic diagram showing the data pre-processing chain is given in Figure 2.

The Level 1b Eagle imagery required geo-correction in order to geometrically rectify and geo-locate the imagery to the UTM projection (zone 29 N) using the WGS84 Earth ellipsoid model. The level 1b images were processed using the FLAASH (Fast Line-of-sight Atmospheric Analysis of Spectral Hypercubes) tool of ENVI 4.7 for atmospheric correction. The FLAASH model utilizes different parameters for atmospheric correction including aerosol content, sensor altitude, ground elevation, pixel size, field of view, atmospheric model, water retrieval, wavelength calibration, zenith angle,

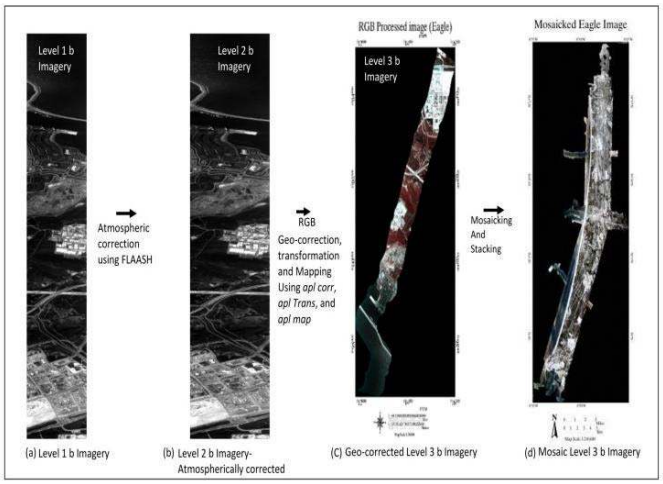

Fig. 2. Main pre processing steps for the hyperspectral imagery (a) level 1b image strips were (b) atmospherically corrected using FLAASH module, (c) geo-corrected, mapped and then (d) mosaicked and stacked together to generate a single seamless image of the study area.

azimuth angle, etc FLAASH accurately compensates for atmospheric effects such as the amount of water vapor, aerosols, and scene visibility. As direct measurements of these atmospheric effects are rarely available, FLAASH infers them from their imprints on the hyperspectral radiance data. FLAASH uses these properties to estimate land surface reflectance using highly accurate models of atmospheric radiation transfer [39].

The input data for FLAASH requires its units to be in μW/cm^2*nm*sr. The scale factor for this conversion is:

$$(Integer\ Radiance image/Scale\ factor) = Floating\ point\ radiance image\ [\mu W/cm^2 * nm * sr]$$

The scale factor should be constant for all bands. Other factors used as input for the atmospheric correction were latitude/longitude, sensor altitude, ground elevation, pixel size, flight date, flight time (GMT), aerosol model, water retrieval, atmospheric model (based on latitudinal and seasonal dependence), initial visibility etc. The aerosol model used in the present study was the maritime aerosol model and the atmospheric model was mid-latitude summer model.

The Level 2 files were geo-corrected for roll, pitch and yaw with the *apl corr* software to produce Level 2b imagery. Utilizing the appended aircraft navigation information from the navigation file and a 4 m DEM generated from the LiDAR first returns, *apl tran* was used to determine the geographic location of every pixel on the ground and then *apl map* to resample the pixels using the nearest-neighbor algorithm to generate a 2 m raster image (*.bil* format) for each flight-line. The Eagle imagery (level 1) has 255 bands with wavelength 399 nm to 1098 nm, but the first and last bands (399nm/1098nm) were removed during processing due to noise. Band 1 and Band 255 were removed from the dataset as these are severely affected by atmospheric scattering [40]. The Hawk image does not have any bad bands. Therefore, any subsequent pre-processing steps

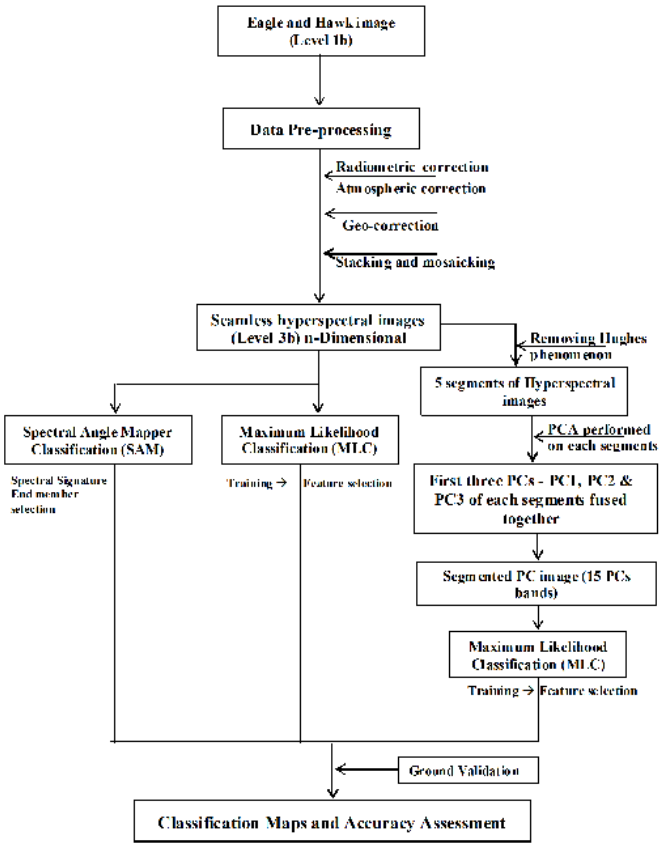

Fig. 3. Flowchart of the data processing methodology.

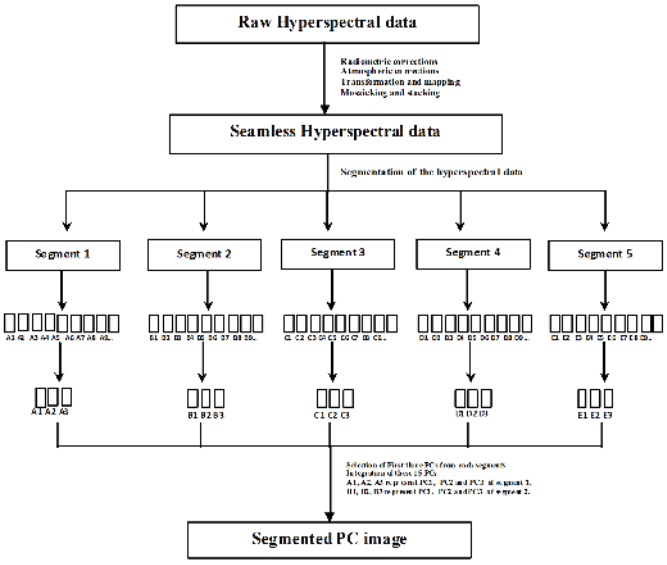

Fig. 4. Flowchart of segmented PC generation.

were only applied to Eagle bands 2–254. Each strip of Eagle data was mosaicked pixel by pixel to generate a final seamless image composite. Similarly, the Hawk data were processed to the same geometry and stacked with the Eagle imagery.

B. PCA and Segmented PCA

Before image classification, a segmented PCA was performed. It uses the attributes of the image histograms and

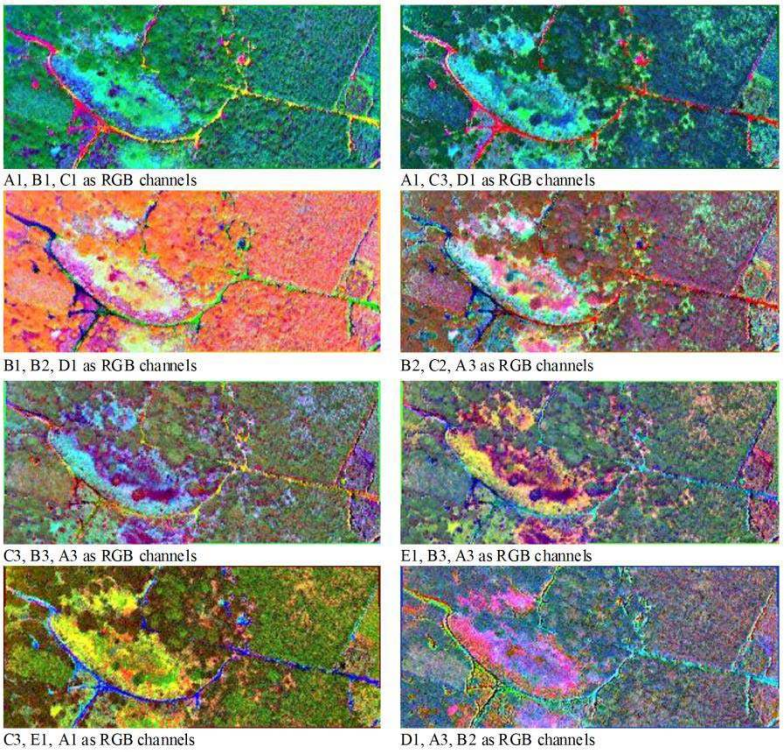

Fig. 5. Different red, blue, green channel combinations of the 15 fused segmented PCs (for A1, A2, A3, B1 etc. refer to Table I).

TABLE I
SEGMENTATION OF HYPERSPECTRAL DATA FROM PCA WITHIN FIVE SPECTRAL DATA SEGMENTS

Hyperspectral segment	Band range based on histograms statistics	Wavelength range	Total no. of PCs	First three PCs (named as)	No. of selected PCs
Segment 1	1-48	399.97-506.15 nm	48	A1- A2-A3	3
Segment 2	49-98	506.15-623.48 nm	50	B1-B2-B3	3
Segment 3	99-142	623.48-728.31 nm	44	C1-C2-C3	3
Segment 4	142-249	701.99 -988.37 nm	107	D1-D2-D3	3
Segment 5	16-212 (Hawk range)	1002.3 –2238.71 nm	196	E1-E2-E3	3
Total PCs selected to generate segmented image					15

wavelengths as illustrated in Figure 4. The segmented PCA approach is utilized to calculate a dataset of reduced dimensionality as input for the maximum likelihood classifier. In order to increase the classification performance, the segmented PCA technique is used to remove redundant bands without losing significant information. A PCA was applied to the 5 different segments of the hyperspectral bands. The first 3 PCs of each of the 5 segments were combined to generate an image with 15 PC bands as shown in Figure 5. The 15 segmented PC bands contain most of the variability of the original 253 Eagle bands and 256 Hawk bands. Thus, almost all of the hyperspectral information is retained and band redundancy and data volume are reduced.

The different PCs are shown in Figure 5 as RGB channel combinations which clearly show the retention of the spectral information as well as visually distinct feature classes. The spectrally segmented PCA results for the 5 different spectral segments are shown in Table I. The higher orders PCs were discarded because they contain mostly noise (eigenvalue < 1). By combining the first 3 PCs from each of the 5 segmented datasets, 15 PC bands contain most of the spectral information

TABLE II
EIGENVALUES FOR THE FIRST THREE PCS DERIVED FROM THE SEGMENTED PCA OF THE HYPERSPECTRAL IMAGE

	PC1	PC2	PC3
Eigenvalues	216.91	33.57	2.03
Variance (%)	85.40	13.22	0.80
Cumulative Variance (%)	85.40	98.62	99.42

of the original hyperspectral data (Figure 4). In the segmented PCA, the hyperspectral bands are subdivided into spectral segments based on band histogram statistics and wavelengths as shown in Table I. On each segment of hyperspectral data bands, a PCA is performed to generate the same number of PCs as the number of input bands (Table I and Figure 4). The first 3 PCs with the highest eigenvalues within each segment (A1, A2, A3, B1, B2, B3…) are fused together to generate the segmented PC datasets. The first 3 PCs were chosen from each segment and fused together to generate the segmented PCs dataset which represent 99.42% of the information content. Different RGB combinations of the segmented PCs are shown

TABLE III
OVERALL ACCURACY AND KAPPA COEFFICIENT FOR MLC, SAM FOR HYPERSPECTRAL IMAGE AND MLC OBTAINED FOR THE CLASSIFIED SEGMENTED PCA IMAGES

	Classifier techniques	Overall Accuracy (%)	Kappa statistics
1	SAM on Hyperspectral data	67.5	0.60
2	MLC on Hyperspectral data	89.67	0.87
3	MLC on Segmented PCA	96.38	0.95

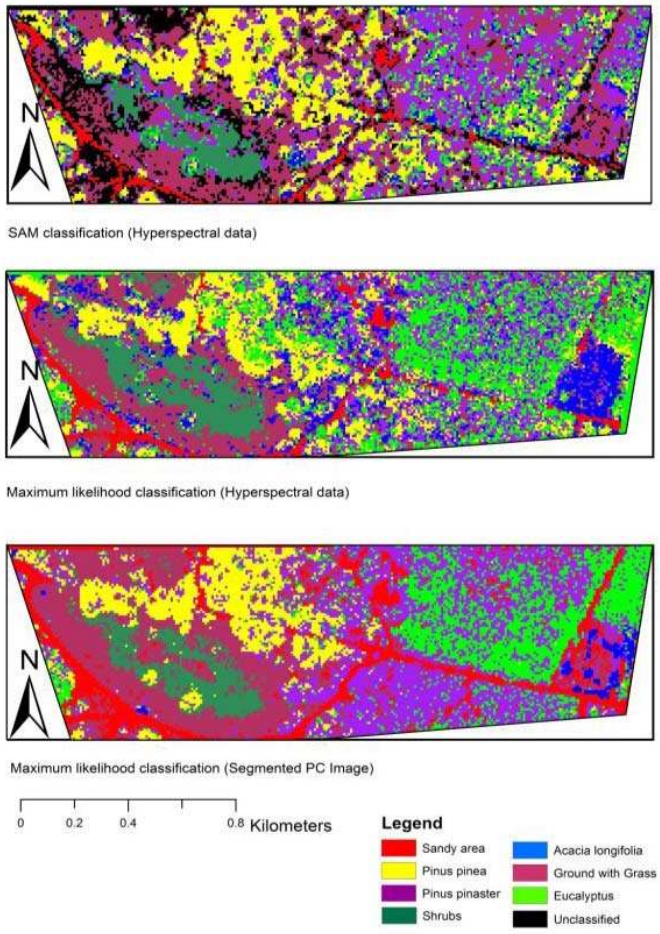

Fig. 6. Classification maps generated using three different classifier techniques. (a) Spectral angle mapper. (b) Maximum likelihood classifier performed on hyperspectral image. (c) Maximum likelihood classifier performed on segmented fused PCs.

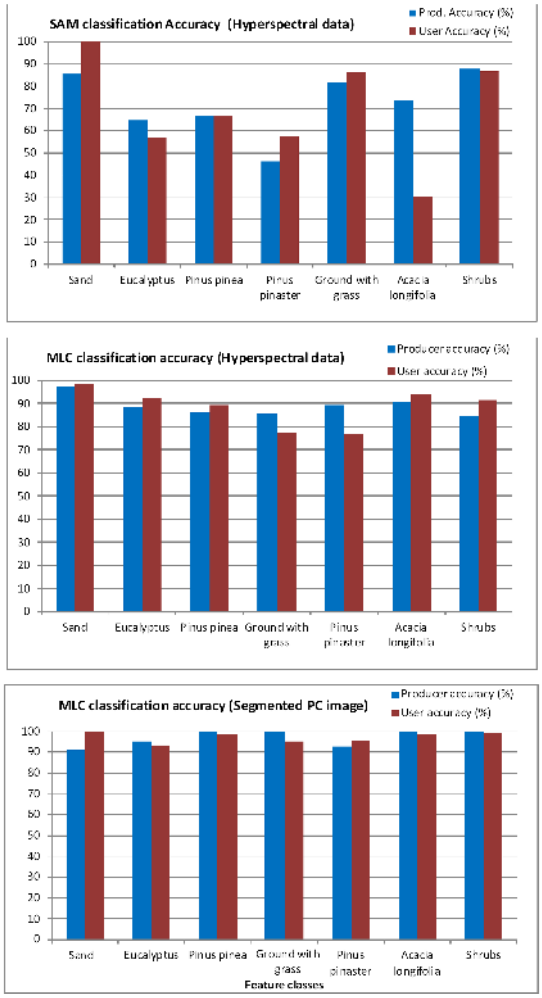

Fig. 7. Graph showing the classification accuracy of the SAM, MLC, and MLC on segmented PCA.

in Figure 5, which clearly enhances the visual interpretation and distinguishes different features. Thereafter, MLC was applied to the 15 segmented PCs. A schematic flowchart of the methodology is shown in Figure 3.

C. Classification Steps

Two classification approaches (Maximum Likelihood classification [41] and Spectral Angle Mapper [42]) were applied to have a baseline comparison for the segmented PCA results. The original mosaicked hyperspectral Eagle and Hawk images were used in the MLC approach. With the aid of training samples, a supervised MLC was performed. In addition, the spectral signatures and *a priori* knowledge of tree species another classified map was produced using SAM.

IV. RESULTS

The classification results for the hyperspectral dataset are shown in Figure 6. The statistical accuracy analysis results of the classifications are given in Table III and Figure 6. The overall accuracy of the MLC of the segmented PC images is significantly higher than for the SAM and MLC approaches applied to the hyperspectral data (Table III). The SAM classification is reliant on spectral image characteristics which can be influenced by the 'Hughes phenomenon' for high-dimensional data. The MLC performed on the segmented PCA bands reduces the 'Hughes phenomenon'. The MLC and SAM classification accuracies for the datasets are presented in Table II. User's and producer's accuracy for different tree species and feature classes were presented in Figure 7.

The accuracy of the MLC based on the segmented PCA is 96.38%, which is much higher than for the MLC classification of the original hyperspectral data (89.67%) and SAM (67.5%). The κ coefficient confirms the superior performance of the MLC on the segmented PC image over the SAM and MLC classifications of the hyperspectral data. The κ coefficient for the three classification approaches gives the same order of classification performance of the three classifier techniques (Table III). The results of the 3 different classification techniques are shown in Figure 6, Figure 7 and Table III.

The PCs of the segmented PC image were uncorrelated containing more than 99% of the information of the original hyperspectral image. Different PC combinations of the segmented PC image were used for visual display using three bands displayed as the red, green and blue channels (RGB channels in Figure 5). The various RGB combinations of the segmented PC images provide visual distinctions between land cover and forest types and other features. This process enhances the color contrast by providing visual clarity for image interpretation, thus helping in selecting the training samples used during classification. These distinctive features in the RGB images were not visible in different band combinations of the original hyperspectral images.

V. Discussion and Conclusion

Tree species classification from hyperspectral imagery is of limited accuracy if the data dimensionality is not reduced, because the 'Hughes phenomenon' leads to a loss of accuracy if too many bands are added. This study explores the classification accuracy achievable from hyperspectral data using the segmented PCA approach. It compares this approach to the SAM and MLC methods of the original hyperspectral data. The classification accuracy and κ coefficient are much higher for the segmented PCA (>96%; $\kappa = 0.95$) than for the other methods when validated with ground control points. The conclusions from this study are:

- Segmented PCA based on data normalization using histogram attributes reduces the dimensionality of the hyperspectral imagery while increasing the classification accuracy.
- The MLC of the segmented PCA produces much more accurate tree species maps than the MLC and SAM classifiers.
- 15 bands of the first 3 PCs of the 5 segments from the full hyperspectral dataset contained >99% of the original spectral variance.
- Compression techniques like segmented PCA to reduce the hyperspectral image dimensionality lead to much improved information content by reducing redundancy of very similar spectral bands.

Some authors have shown conventional parametric classification approaches, i.e. MLC as being limited in their ability to classify high dimensionality data [43], [44]. Although this makes MLC unsuitable for raw hyperspectral data, this study shows that MLC can be used after reducing the dimensions of the hyperspectral imagery. The segmented PCA method enhances the contrast of the imagery and provides better visual clarity for image interpretation, thus helping in selecting the training samples used during MLC. Thus, it provides better training samples and better accuracy [10]–[12]. MLC was chosen in the present study as a classifier after reducing the dimensionality of the hyperspectral data using the segmented PCA approach.

Finally, the segmented PCA approach used in the present study will be helpful for hyperspectral analysis by reducing the multidimensional data to smaller dimensionality for image processing while retaining most of the information. This image compression technique can be used with other classification algorithms to achieve accurate tree species identification results by reducing data dimensionality and data volume. This classification approach can be used for other applications like urban mapping, land cover mapping, plant stress detection due to its visual enhancement, fire scar mapping etc.

Acknowledgment

The authors would like to thank André Große-Stoltenberg, Tillmann Buttschardt (University of Münster, Germany) and Katurah Z. Smithson staff University of Leicester for their help during field work. We would like to extend our sincere gratitude to the Airborne Research and Survey Facility (ARSF, Gloucester, U.K.) and Natural Environment Research Council (NERC) for acquiring airborne data under EUFAR project EUFAR11/06 in 2011. The data were provided by André Große-Stoltenberg. P.C. Pandey was supported by the Association of Commonwealth Universities, (INCS-2011-155 commonwealth fellowship). H. Balzter was supported by the Royal Society Wolfson Research Merit Award, 2011/R3. The authors would like to thank Mark Warren and Emma Carolan (Plymouth Marine Laboratory, Plymouth) for their help in hyperspectral data processing.

References

[1] M. A. Cochrane, "Using vegetation reflectance variability for species level classification of hyperspectral data," *Int. J. Remote Sens.*, vol. 21, no. 10, pp. 2075–2087, Jul. 2000.

[2] G. P. Asner *et al.*, "Invasive species detection in Hawaiian rainforests using airborne imaging spectroscopy and LiDAR," *Remote Sens. Environ.*, vol. 112, no. 5, pp. 1942–1955, May 2008.

[3] Z. Hao, H. Hao, Y. Xu-Guo, Z. Ke-Feng, and G. Yi, "Estimation of above-ground biomass using HJ-1 hyperspectral images in Hangzhou Bay, China," in *Proc. Int. Conf. Inf. Eng. Comput. Sci. (ICIECS)*, Dec. 2009, pp. 1–4.

[4] H. Cetin, "Comparison of spaceborne and airborne hyperspectral imaging systems for environmental mapping," in *Proc. 20th ISPRS Congr., Tech. Commission VII, Istanbul, Turkey*, 2004, pp. 1306–1313.

[5] Y. Kim, D. M. Glenn, J. Park, H. K. Ngugi, and B. L. Lehman, "Hyperspectral image analysis for plant stress detection," in *Proc. Annu. Int. Meeting Amer. Soc. Agricult. Biolo. Eng. (ASABE)*, Pittsburgh, PA, USA, 2010, pp. 1–11.

[6] P. Kumar, L. K. Sharma, P. C. Pandey, S. Sinha, and M. S. Nathawat, "Geospatial strategy for tropical forest-wildlife reserve biomass estimation," *IEEE J. Sel. Topics Appl. Earth Observat. Remote Sens.*, vol. 6, no. 2, pp. 917–923, Apr. 2013.

[7] S. K. Singh, P. K. Srivastava, M. Gupta, J. K. Thakur, and S. Mukherjee, "Appraisal of land use/land cover of mangrove forest ecosystem using support vector machine," *Environ. Earth Sci.*, vol. 71, no. 5, pp. 2245–2255, Mar. 2014.

[8] M. Frank, P. Zhihong, B. Raber, and C. Lenart, "Vegetation management of utility corridors using high-resolution hyperspectral imaging and LiDAR," in *Proc. 2nd Workshop Hyperspectral Image Signal Process. Evol. Remote Sens. (WHISPERS)*, Jun. 2010, pp. 1–4.

[9] M. Schaepman, S. Ustin, A. Plaza, T. Painter, J. Verrelst, and S. Liang, "Earth system science related imaging spectroscopy—An assessment," *Remote Sens. Environ.*, vol. 113, pp. S123–S137, Sep. 2009.

[10] N. Baatuuwie and L. Van Leeuwen, "Evaluation of three classifiers in mapping forest stand types using medium resolution imagery: A case study in the Offinso Forest District, Ghana," *African J. Environ. Sci. Technol.*, vol. 5, no. 1, pp. 25–36, Jan. 2011.
[11] E. L. Hunter and C. H. Power, "An assessment of two classification methods for mapping Thames Estuary intertidal habitats using CASI data," *Int. J. Remote Sens.*, vol. 23, no. 15 pp. 2989–3008, Nov. 2002.
[12] H. Z. M. Shafri, A. Suhaili, and S. Mansor, "The performance of maximum likelihood, spectral angle mapper, neural network and decision tree classifiers in hyperspectral image analysis," *J. Comput. Sci.*, vol. 3, no. 6, p. 419, Jun. 2007.
[13] P. M. Mather, B. Tso, and M. Koch, "An evaluation of Landsat TM spectral data and SAR-derived textural information for lithological discrimination in the Red Sea Hills, Sudan," *Int. J. Remote Sens.*, vol. 19, no. 4, pp. 587–604, Mar. 1998.
[14] A. O. Onojeghuo and G. A. Blackburn, "Mapping reedbed habitats using texture-based classification of QuickBird imagery," *Int. J. Remote Sens.*, vol. 32, no. 23, pp. 8121–8138, Sep. 2011.
[15] A. O. Onojeghuo and G. A. Blackburn, "Optimising the use of hyperspectral and LiDAR data for mapping reedbed habitats," *Remote Sens. Environ.*, vol. 115, no. 8, pp. 2025–2034, Aug. 2011.
[16] K. Jusoff, "Land use and cover mapping with airborne hyperspectral imager in Setiu, Malaysia," *J. Agricult. Sci.*, vol. 1, no. 2, pp. 120–131, 2009.
[17] G. P. Petropoulos, K. Arvanitis, and N. Sigrimis, "Hyperion hyperspectral imagery analysis combined with machine learning classifiers for land use/cover mapping," *Expert Syst. Appl.*, vol. 39, no. 3, pp. 3800–3809, Feb. 2012.
[18] P. Gong, R. Pu, and J. R. Miller, "Correlating leaf area index of ponderosa pine with hyperspectral CASI data," *Can. J. Remote Sens.*, vol. 18, pp. 275–282, Jan. 1992.
[19] S. Pe'eri, J. R. Morrison, F. Short, A. Mathieson, A. Brook, and P. Trowbridge, "Microalgae and eelgrass mapping in great bay estuary using AISA hyperspectral imagery," New Hampshire, NH, USA: Environmental Protection Agency 2008.
[20] P. H. Rosso, S. L. Ustin, and A. Hastings, "Mapping marshland vegetation of San Francisco Bay, California, using hyperspectral data," *Int. J. Remote Sens.*, vol. 26, pp. 5169–5191, Dec. 2005.
[21] M. L. Clark, D. A. Roberts, and D. B. Clark, "Hyperspectral discrimination of tropical rain forest tree species at leaf to crown scales," *Remote Sens. Environ.*, vol. 96, nos. 3–4, pp. 375–398, Jun. 2005.
[22] F. Tsai, E.-K. Lin, and K. Yoshino, "Spectrally segmented principal component analysis of hyperspectral imagery for mapping invasive plant species," *Int. J. Remote Sens.*, vol. 28, no. 5, pp. 1023–1039, Mar. 2007.
[23] A. A. Green, M. Berman, P. Switzer, and M. D. Craig, "A transformation for ordering multispectral data in terms of image quality with implications for noise removal," *IEEE Trans. Geosci. Remote Sens.*, vol. 26, no. 1, pp. 65–74, Jan. 1988.
[24] L. M. Bruce, C. H. Koger, and J. Li, "Dimensionality reduction of hyperspectral data using discrete wavelet transform feature extraction," *IEEE Trans. Geosci. Remote Sens.*, vol. 40, no. 10, pp. 2331–2338, Oct. 2002.
[25] V. Karathanassi, P. Kolokousis, and S. Ioannidou, "A comparison study on fusion methods using evaluation indicators," *Int. J. Remote Sens.*, vol. 28, no. 10, pp. 2309–2341, May 2007.
[26] P.-H. Hsu and Y.-H. Tseng, "Feature extraction for hyperspectral image," in *Proc. 20th Asian Conf. Remote Sens.*, pp. 405–410, 1999.
[27] R. Bellman, *Adaptive Control Processes: A Guided Tour*. Princeton, NJ, USA: Princeton Univ. Press, 1961.
[28] R. Hughes, "On the mean accuracy of statistical pattern recognizers," *IEEE Trans. Inf. Theory*, vol. 14, no. 1, pp. 55–63, Jan. 1968.
[29] R. Nishii, S. Kusanobu, and N. Nakaoka, "Hughes phenomenon in the spatial resolution enhancement of low resolution images and derivation of selection rule for high resolution images," in *Proc. IEEE Int. Geosci. Remote Sens., Remote Sens.-A Sci. Vis. Sustain. Develop.*, vol. 2. Aug. 1997, pp. 649–651.
[30] D. A. Landgrebe, *Signal Theory Methods in Multispectral Remote Sensing*. New York, NY, USA: Wiley, 2003.
[31] M. C. Alonso, J. A. Malpica, and A. Martínez de Agirre, "Consequences of the Hughes phenomenon on some classification Techniques," presented at *Annu. Conf. (ASPRS)*, Milwaukee, WI, USA, May 2011.
[32] D. W. Scott, "The curse of dimensionality and dimension reduction," in *Multivariate Density Estimation: Theory, Practice, and Visualization*. New York, NY, USA: Wiley, 1992, pp. 195–217.
[33] A. Plaza, P. Martínez, J. Plaza, and R. Pérez, "Dimensionality reduction and classification of hyperspectral image data using sequences of extended morphological transformations," *IEEE Trans. Geosci. Remote Sens.*, vol. 43, no. 3, pp. 466–479, Mar. 2005.
[34] K. Sundseth. (2000, Apr. 12). *Natura 2000 in the Mediterranean Region, European Commission*. [Online]. Available: http://ec.europa.eu/environment/nature/info/pubs/docs/biogeos/Mediterranean.pdf
[35] G. Scarascia-Mugnozza, H. Oswald, P. Piussi, and K. Radoglou, "Forests of the Mediterranean region: Gaps in knowledge and research needs," *Forest Ecol. Manag.*, vol. 132, no. 1, pp. 97–109, Jun. 2000.
[36] F. Ortenberg, "Hyperspectral sensor characteristics: Sirborne, space borne, hand-held and truck-mounted; integration of hyperspectral data with LiDAR," in *Hyperspectral Remote Sensing of Vegetation*, P. S. Thenkabail, J. G. Lyon, and A. Huete, Eds. Boca Raton, FL, USA: CRC Press, 2011.
[37] T. M. Lillesand, R. W. Kiefer, and J. W. Chipman, *Remote Sensing & Image Interpretation*. New York, NY, USA: Wiley, 2004.
[38] *Airborne Processing Library Getting Started With APL—Command Line*, Natural Environment Research Council, Oxford, U.K., Aug. 2012.
[39] S. M. Adler-Golden *et al.*, "Atmospheric Correction for Short-wave Spectral Imagery Based on MODTRAN4," in *Proc. SPIE Imaging Spectrometry*, 1999, pp. 61–69.
[40] V. R. Copley, "Debris provenance mapping in braided drainage using remote sensing," *Geological Soc., London, Special Publications*, vol. 75, no. 1, pp. 405–412, 1993.
[41] J. A. Richards and X. Jia, *Remote Sensing Digital Image Analysis—An Introduction*, 4th ed. Berlin, Germany: Springer-Verlag, 1999.
[42] F. A. Kruse *et al.*, "The spectral image-processing system (sips)—Interactive visualization and analysis of imaging spectrometer data," *Remote Sens. Environ.*, vol. 44, nos. 2–3, pp. 145–163, May/Jun. 1993.
[43] J. A. Benediktsson, P. H. Swain, and O. K. Ersoy, "Neural network approaches versus statistical-methods in classification of multisource remote-sensing data," *IEEE Trans. Geosci. Remote Sens.*, vol. 28, no. 4, pp. 540–552, Jul. 1990.
[44] T. G. Jones, N. C. Coops, and T. Sharma, "Assessing the utility of airborne hyperspectral and LiDAR data for species distribution mapping in the coastal Pacific Northwest, Canada," *Remote Sens. Environ.*, vol. 114, no. 12, pp. 2841–2852, Dec. 2010.

Prem Chandra Pandey (M'12) received the B.Sc. degree and the M.Sc. degree in environmental sciences from Banaras Hindu University, Varanasi, India, in 2005 and 2007, respectively, and the M.Tech. degree in remote sensing from the Birla Institute of Technology, Ranchi, India, in 2009. He was a recipient of the Commonwealth Scholarship (2011) for pursuing doctorate in Geography at the University of Leicester, Leicester, U.K. He is currently a Post-Graduate Researcher in Remote Sensing Technology with the Centre for Landscape and Climate Research, University of Leicester.

Mr. Pandey is a member of the Association of American Geographers, the American Geophysical Union, the Indian Society of Remote Sensing, the International Society for Optics and Photonics (SPIE), and the Indian Society of Geomatics. His research interests include urban environment, forest mapping using airborne hyperspectral and Lidar data.

Nicholas J. Tate received the bachelor's degree in geography from Durham University, Durham, U.K., in 1986, and the Ph.D. degree from the School of Environmental Sciences, University of East Anglia, Norfolk, U.K., in 1996.

He has been with the Department of Geography, University of Leicester, Leicester, U.K., since 1999, where he is currently a Senior Lecturer. He is the Director of the Leicester LiDAR Research Unit, and also Director of Post-Graduate Research with the College of Science and Engineering. From 1994 to 1998, he was a Lecturer with the School of Geography, Queen's University Belfast, Belfast, U.K. His research interests range from the mathematical characterization and representation of topographic surfaces to the use of airborne and, most recently, terrestrial LiDAR for surface generation. He is currently the Chair of the RSPSoc LiDAR SIG and is on the editorial board of the journal *Transactions in GIS*.

Heiko Balzter received the Dipl.-Ing.Agr. (equivalent to M.Sc.) and the Dr.Agr. (Ph.D.) degrees from Justus-Liebig-University, Giessen, Germany, in 1994 and 1998, respectively.

He is a Research Professor and the Director of the Centre for Landscape and Climate Research at the University of Leicester, Leicester, U.K. Before joining the University of Leicester, he was Head of the Section for Earth Observation at the Centre for Ecology and Hydrology, Monks Wood, U.K., where he worked from 1998 to 2006. His research interests include interactions of the water cycle with ecosystems across multiple spatial and temporal scales, pressures from climate change and land use change on ecosystem services, and the effects of spatial patterns and processes upon biological populations in evolving 3-D landscapes.

Prof. Balzter is a member of the American Geophysical Union, the British Ecological Society, the Remote Sensing and Photogrammetry Society, and the Chartered Management Institute, and a fellow of the Royal Geographical Society and the Royal Statistical Society. He is a coordinator of the European Centre of Excellence in Earth Observation Research Training GIONET, and was a recipient of the 2012 Royal Society Wolfson Research Merit Award. He received the President's Cup for the Best Paper at the 2009 Annual Remote Sensing and Photogrammetry Society Conference, and serves on the International Geosphere/Biosphere Program U.K. National Committee, the European Space Sciences Committee of the European Science Foundation, the LULUCF Scientific Steering Committee for the Department for Energy and Climate Change, the AATSR Science Advisory Group to Department for Environment, Food and Rural Affairs, and the Natural Environment Research Council Peer Review College.